Giant magnetic proximity effect in amorphous layered magnets

K. A. Thórarinsdóttir,[1] H. Palonen,[2] G. K. Palsson,[2] B. Hjörvarsson,[2] and F. Magnus[1,2,*]
[1]*Science Institute, University of Iceland, Dunhaga 3, IS-107 Reykjavik, Iceland*
[2]*Department of Physics and Astronomy, Uppsala University, Box 530, SE-75121 Uppsala, Sweden*

(Received 12 December 2018; revised manuscript received 8 April 2019; published 21 May 2019)

Here we study the magnetic proximity effect in amorphous layered magnets of alternating high- and low-T_c materials using magnetometry and polarized neutron reflectivity. By altering the thickness of either the high- or low-T_c layer we are able to extract the induced magnetic moment in the low-T_c layer directly and study how it scales with thickness. We observe that the ordering temperature of the low-T_c layer is enhanced and above which a second magnetically ordered state with a very large extension is observed. This induced magnetic state survives to a temperature at least three times that of the ordering temperature of the low-T_c layer and the induced magnetization is approximately constant throughout at least a 10-nm-thick layer. The induced magnetic region within the low-T_c layer does not depend on the thickness of the adjacent high-T_c layer.

DOI: 10.1103/PhysRevMaterials.3.054409

I. INTRODUCTION

The magnetic proximity effect refers to an induced magnetic ordering in an intrinsically nonmagnetic material which is brought about by proximity to a magnetic material [1,2]. It is typically observed in composite or layered structures, where one component is ferromagnetic (FM) or antiferromagnetic (AFM) and the other is paramagnetic (PM) or has a lower ordering temperature [3]. The influence of such a proximity effect can be diverse. In FM-PM systems a magnetization can be induced in the PM material and in FM-FM or FM-AFM systems the ordering temperature (T_c or T_N) can be enhanced [4–6]. The induced magnetization can in turn result in nonoscillatory interlayer exchange coupling across metallic spacers [7] as well as spring-magnetic behavior and long-range exchange bias through intrinsically paramagnetic layers [5].

Nanoscale magnetic devices such as magnetic memory, sensors, and logic devices are typically composed of layers of coupled magnetic and nonmagnetic materials [8,9]. Magnetic proximity effects will inevitably influence the performance of such devices and must be taken into account in their design [3]. Layering of different types of magnetic materials is also a powerful way to tune or enhance their overall magnetic properties [10]. In this context, the proximity effect can, for example, be used to increase the ordering temperature of dilute magnetic semiconductors [11], control interlayer coupling [5] or induce ferromagnetism or more complex spin textures in topological insulators [12–14]. Therefore, it is important to gain a better understanding of the magnetic proximity effect and determine its size and extension in technologically important systems.

The proximity effect arises because of magnetic interactions between atoms across the interface and hybridization of interface states [2]. It has generally been considered to be short-ranged, typically extending only a few atomic layers into the nonmagnetic material [2,3,15]. For example, in the much studied Fe/V system the magnetic moment in the V has an exponential decay length of approximately 0.3 nm [15] but by replacing the V with an FeV alloy the decay length can be extended to 1.7 nm [16]. A somewhat larger proximity effect is found in high susceptibility paramagnets such as Pd and Pt where the induced magnetization can extend up to a few nanometers into the paramagnet [17–19]. Recently, however, it has been shown indirectly that in amorphous heterostructures the effect can extend several tens of nanometers into the nonmagnetic material [5]. This is achieved by tuning the composition of the amorphous alloys such that they are on the verge of ferromagnetism or have a low ferromagnetic ordering temperature. By using amorphous materials it is possible to tune the intrinsic ordering temperature without significantly affecting the interface structure since there is no lattice mismatch at the interfaces [20,21]. In addition, the density modulations inherent in such disordered alloys could contribute to the long range of the proximity effect [22,23].

Here we study the magnetic proximity effect in amorphous multilayers which are composed of alternating high- and low-T_c layers by a combination of magnetometry and polarized neutron reflectivity. This allows us to measure directly the magnetization which is induced in the low-T_c layers above their intrinsic ordering temperature and determine how the region of induced magnetization scales with the layer thickness. The results show that proximity effects can induce an almost constant magnetization with a remarkably long extension in an intrinsically paramagnetic amorphous material.

II. EXPERIMENTAL METHODS AND DESIGN

The samples were grown at room temperature by dc magnetron sputtering in a sputtering chamber with a base pressure below 5×10^{-10} Torr. The sputtering gas was Ar of 99.9999% purity and the growth pressure was 2.0 mTorr. Si(100) substrates with the native oxide layer were used. The substrates

*fridrikm@hi.is

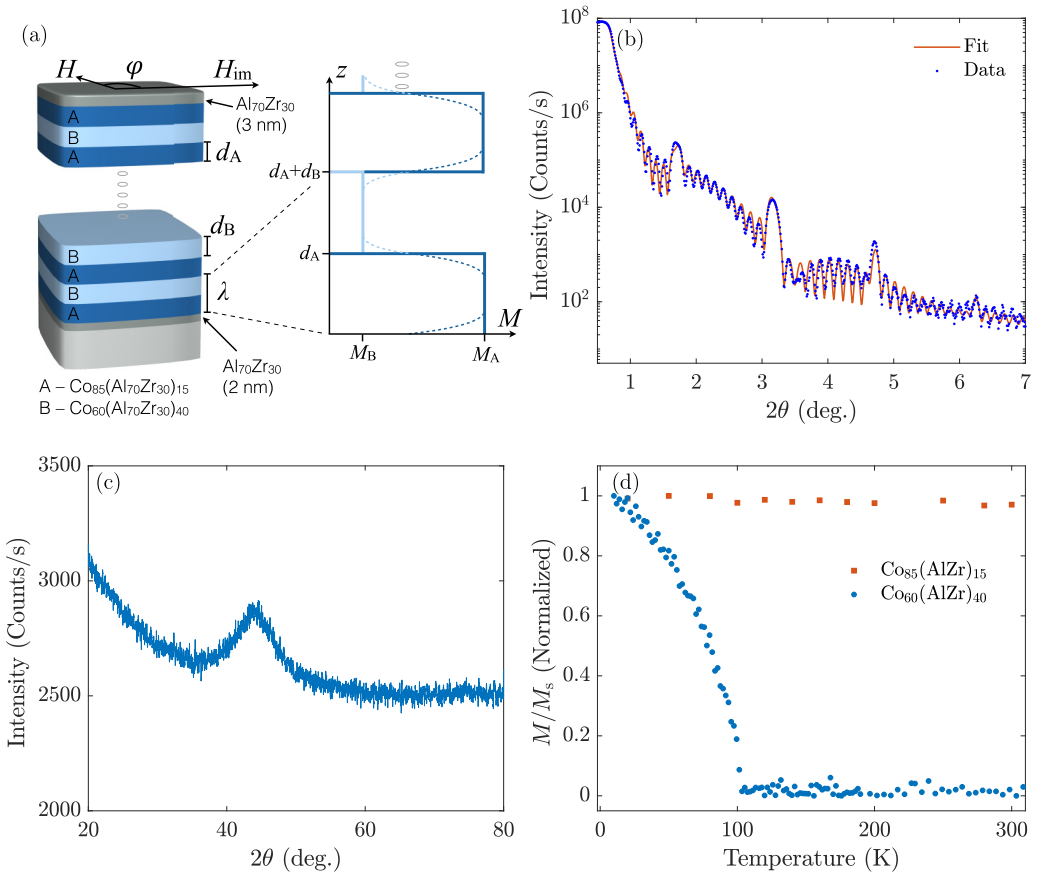

FIG. 1. (a) A schematic of the sample structure (left) and the magnetization profile of one bilayer, below T_c^B (right). The solid lines are a simple constant magnetization approximation, whereas the dashed lines represent a smoothly varying magnetization across the interfaces. (b) x-Ray reflectivity of the multilayer with $d_B = 5$ nm and $d_A = 1$ nm including a fit. (c) A representative grazing incidence x-ray diffraction scan of a multilayer sample showing a broad characteristic amorphous peak. (d) Remanent magnetization for $Co_{85}(Al_{70}Zr_{30})_{15}$ (layer A) and $Co_{60}(Al_{70}Zr_{30})_{40}$ (layer B) showing an ordering temperature of $T_c^B = 103 \pm 5$ K for the $Co_{60}(Al_{70}Zr_{30})_{40}$. The data are normalized to the saturation magnetization at 10 K.

were annealed in vacuum at 550 °C for 30 minutes prior to growth. First, a 2-nm-thick buffer layer of $Al_{70}Zr_{30}$ was deposited on the substrate from an $Al_{70}Zr_{30}$ alloy target (purity 99.9%). Subsequently, a multilayer of $Co_{85}(Al_{70}Zr_{30})_{15}$ (layer A) and $Co_{60}(Al_{70}Zr_{30})_{40}$ (layer B) was grown by cosputtering from Co (purity 99.9%) and $Al_{70}Zr_{30}$ targets, always beginning and ending with a $Co_{85}(Al_{70}Zr_{30})_{15}$ layer. Between layers, the shutters in front of all magnetrons were closed momentarily while the power applied to the Co magnetron was changed to obtain the desired composition. The composition was determined by careful rate calibrations for each magnetron. All samples were capped with a 3-nm layer of AlZr. The sample structure is shown schematically in Fig. 1(a). The room temperature growth, choice of compositions, and the use of an $Al_{70}Zr_{30}$ buffer layer ensures that the films are fully amorphous and that the interfaces are sharp [24,25]. x-Ray reflectivity (XRR) and grazing incidence x-ray diffraction (GIXRD) measurements were performed to confirm this. A PANalytical X'pert Pro diffractometer was used, equipped with a Göbel mirror on the incident side and a parallel plate collimator on the diffracted side. Characteristic XRR and GIXRD measurements are shown in Figs. 1(b) and 1(c), respectively. The XRR shows clear multilayer Bragg peaks which arise due to the periodicity in the sample density, as well as Kiessig thickness fringes up to at least $2\theta = 7°$, attesting to the low surface and interface roughnesses. Fitting of the XRR data using the layer model shown in Fig. 1(a) gives interface widths of approximately 0.4-nm rms and confirms that the actual thicknesses agree with the nominal ones. We can therefore rule out intermixing between layers or interlayer coupling due to interface roughness (orange peel coupling). The GIXRD (performed with the incidence angle fixed at $\omega = 1°$) shows a single broad peak centered at approximately $2\theta = 45°$, characteristic of an amorphous structure (see, for example, Ref. [26]).

The difference in cobalt content results in different intrinsic ordering temperatures of layers A and B when grown separately. Layer A has an ordering temperature T_c^A which is well above room temperature, whereas layer B has an ordering temperature of $T_c^B = 103 \pm 5$ K, as shown by the temperature dependence of the remanent magnetization of each layer in Fig. 1(d). Below the ordering temperatures of both layers they are both ferromagnetic but the magnetization of layer B will be significantly lower than that of A, as shown schematically in Fig. 1(a). In the temperature regime between the two ordering temperatures there will be an induced magnetization in the B layer due to the proximity to the A layer but its size, extension, and profile is unknown. In order to study these

factors, two thickness series of the layers were produced: (i) with the layer A thickness fixed at $d_A = 5$ nm and the B-layer thickness d_B in the range 2.5 to 10 nm (hereafter referred to as the B-layer series) and (ii) with the B-layer thickness fixed at 5 nm and the A-layer thickness in the range 1 to 10 nm (hereafter referred to as the A-layer series). In addition, a uniaxial in-plane anisotropy was induced in the A layers by applying a magnetic field of approximately $H_{im} = 0.1$ T during growth [24,25]. The total magnetic moment of the multilayers was measured using vibrating sample magnetometry (VSM) in a longitudinal geometry. Full hysteresis curves were measured parallel to the plane of the films at each temperature and the saturation moment at 20 mT extracted.

Polarized neutron reflectivity (PNR) measurements were carried out on the Super ADAM beamline at the Institut Laue–Langevin to study the magnetization profile of the multilayers. The neutron wavelength was 5.183 Å and the measurements were performed at 120 K (somewhat above T_c^B). A guide field of 1.5–3.0 mT was used to maintain the neutron polarization parallel to the plane of the films and an electromagnet was used to saturate the sample along the in-plane easy axis, which was in all cases parallel to the guide field. The data was normalized by a monitor to account for fluctuations in the neutron flux and to correct for points measured for different lengths of time. A constant slit opening for the entire data set was chosen such that the sample was overilluminated which was corrected for before fitting. Fitting of the data was performed in the GenX software package [27] using the layer model depicted in Fig. 1(a).

III. RESULTS AND DISCUSSION

Representative magnetic hysteresis curves for the multilayers can be seen in Fig. 2(a) where the magnetization is measured at an in-plane angle of $\varphi = 0°$ and $\varphi = 90°$ with respect to the growth field. The uniaxial anisotropy imprinted by the growth field results in a square hysteresis loop for $\varphi = 0°$ (the easy axis) and a linear hysteresis loop with zero remanence along $\varphi = 90°$ (the hard axis). The measurements shown in the figure are for the sample with $d_B = 5$ nm and $d_A = 10$ nm at room temperature but the general shape of the hysteresis curves is the same at all temperatures and for all samples.

The saturation (20 mT) magnetization extracted from such hysteresis loops as a function of temperature is shown in Fig. 2(b) for the B-layer series. For the sample with $d_B = 10$ nm, a clear change in slope dM/dT is seen at approximately 140 K, which is somewhat above the intrinsic ordering temperature of the B layer. This indicates that the multilayer has an ordering temperature that is above T_c^B, although the exact temperature cannot be pinpointed with the current data. For thinner B layers (2.5 nm and 5.0 nm) the magnetization appears to decrease monotonously with increasing temperature and there is no clear sign of a magnetic phase transition. This is strong evidence of a large magnetic proximity effect. However, it is difficult to determine with any certainty from this data presentation how the magnetization of the B layer changes because of the relative size of the magnetization of the A and B layers.

The scaling of the magnetization with d_B gives an insight into the size and extension of the induced magnetization in the

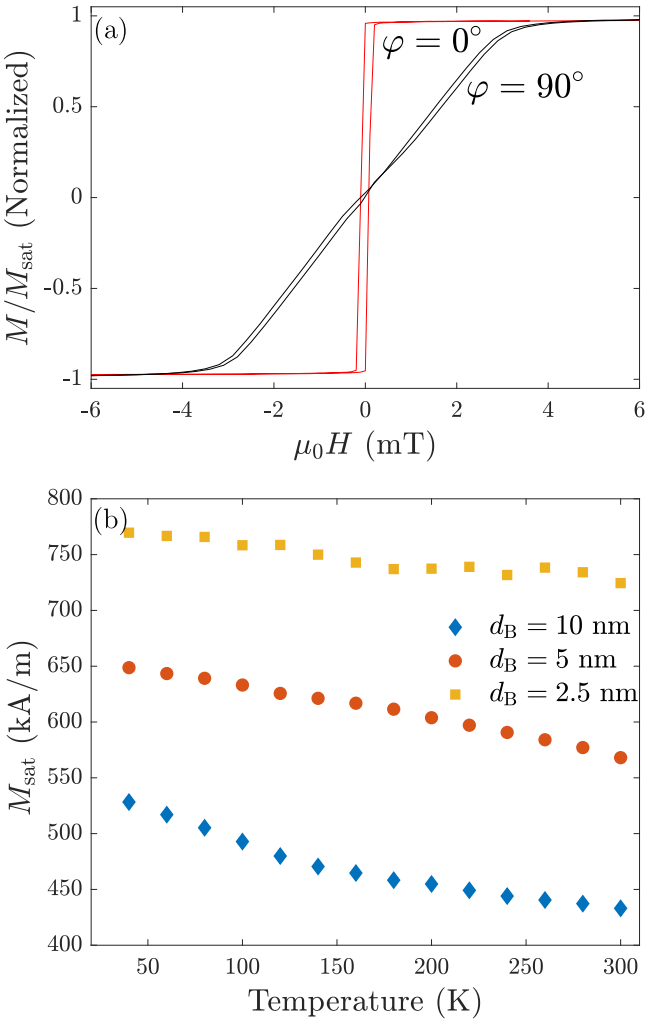

FIG. 2. (a) Room-temperature magnetization, normalized by the saturation magnetization, versus applied in-plane magnetic field for the multilayer with $d_B = 5$ nm and $d_A = 10$ nm. The field is oriented either parallel (red) or perpendicular (black) to the applied growth field, resulting in an easy or hard axis response, respectively. (b) The saturation magnetization of the B-layer thickness series as a function of temperature.

B layer. The simplest model to describe the magnetization of the layers is to assume that it is constant within each layer. This is depicted in Fig. 1(a) with the solid blue lines. In this case, the average magnetization of a bilayer of thickness $\lambda = d_A + d_B$ is given by the weighted average of the magnetization of the two layers, which can be expressed as

$$M_{avg} = d_A(M_A - M_B)\frac{1}{\lambda} + M_B, \quad (1)$$

where M_{avg} is the average saturation magnetization of the bilayer and M_A and M_B the saturation magnetizations of layers A and B, respectively [16].

Figure 3(a) shows the measured magnetization, plotted as a function of the inverse bilayer thickness for the B-layer series. The linear dependence with a nonzero intercept at all temperatures is striking and fully consistent with Eq. (1). The variation in the slope is due only to a variation in the

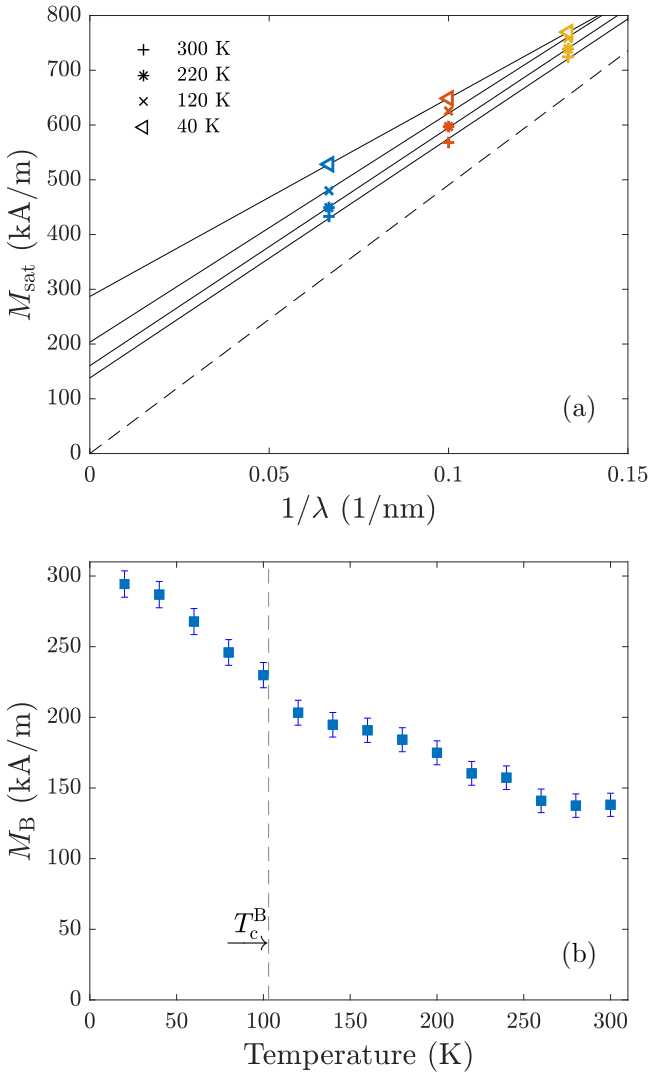

FIG. 3. (a) The saturation magnetization versus the inverse bilayer thickness for a selection of temperatures for the B-layer thickness series. The solid lines are fits to the data and the dashed line is the linear model [Eq. (1)] with M_B set to zero (no proximity effect). (b) The magnetization of the B layer, M_B, extracted from the intercept of the fitted lines in (a). The intercept corresponds to M_B according to the linear model [Eq. (1)].

magnetization of layer B since both M_A and d_A are constant in this thickness series. The slope is positive due to the fact that $M_B < M_A$ and increases with increasing temperature, in line with a decreasing M_B. The intercept yields M_B directly which should reduce to zero above T_c^B in the absence of a proximity effect, as shown by the dashed line in the figure (where we use the measured "bulk" value of M_A). This is clearly not the case, even at room temperature, showing that there is a proximity induced magnetization in layer B at three times its intrinsic ordering temperature. Furthermore, an exponentially decaying profile of the induced magnetization would be expected away from the interfaces [5], which would result in a nonlinear scaling of M with λ^{-1} [16]. This is not observed in Fig. 3(a), meaning that the magnetization is indeed approximately constant throughout the entire thickness of the layer at all temperatures. Therefore, either the decay length is significantly longer than the largest B-layer thickness (10 nm) or the magnetization decays to a constant value with a decay length much smaller than the smallest d_B. This scenario is depicted schematically in Fig. 2(a) with the dashed lines.

The temperature dependence of the magnetization of layer B is shown in Fig. 3(b). The values are extracted from the intercepts of the linear fits in Fig. 3(a). The magnetization decreases with increasing temperature, as expected, but is nonzero at all measured temperatures as previously noted. However, there is a critical point in the curve at a temperature somewhat above T_c^B reminiscent of the ferromagnetic to paramagnetic phase transition which occurs in B on layer its own at T_c^B. This shows the dual impact of the magnetic proximity effect; first, it enhances the ordering temperature of the B layer and, second, it induces a new magnetically ordered state with a very large extension, which survives to much higher temperatures.

This dual impact of the proximity effect is consistent with a previous study of a similar amorphous heterostructure composed of a B layer sandwiched by an A layer and a SmCo hard magnet layer [5]. This study showed that the proximity effect resulted in both spring-magnet behavior and exchange bias but the two had very different temperature dependence and extension. Below the enhanced ordering temperature they had an induced ferromagnetic state with a significant spin stiffness which could sustain a spring-magnet effect. At higher temperatures they had a magnetic state with a significant moment but negligible spin stiffness (a super-paramagnetic-like state) which could cause an exchange bias on an adjacent magnetic layer. In the multilayers studied here we do not have a spring-magnet effect or exchange bias since all layers have a small anisotropy and the structure switches as a whole. However, we are able to detect the induced magnetization directly for the two different magnetic phases. The large extension of the proximity effect and the resulting complex magnetic phase diagram can be explained by the amorphous structure and composition of the films. In general, the hybridization of the $3d$ band of the ferromagnet across the interface will decay rapidly away from the interface on a length scale of a few atomic layers. However, the ordering temperature of the B layer is strongly dependent on the amount of Co and therefore a small increase in the density of states can be sufficient to enhance it significantly. In addition, the inherent local variation in the concentration of the magnetic element within the amorphous alloy means that it will inevitably have local variations in T_c with interconnected regions of high and low magnetic coupling strength [22]. An effective field from the adjacent ferromagnets can therefore polarize the amorphous alloy far above its intrinsic ferromagnetic ordering temperature.

The temperature dependence of the magnetization of the A-layer thickness series is presented in the inset of Fig. 4(a). Note that the sample $d_A = d_B = 5$ nm is common to both thickness series. There is no inflection around T_c^B for any of the samples, and the magnetic moment decreases monotonously. This indicates that the induced magnetization in layer B does not depend on the thickness of the source layer.

The scaling of the magnetization of the A series with λ^{-1} can be seen in Fig. 4(b). Assuming a constant magnetization

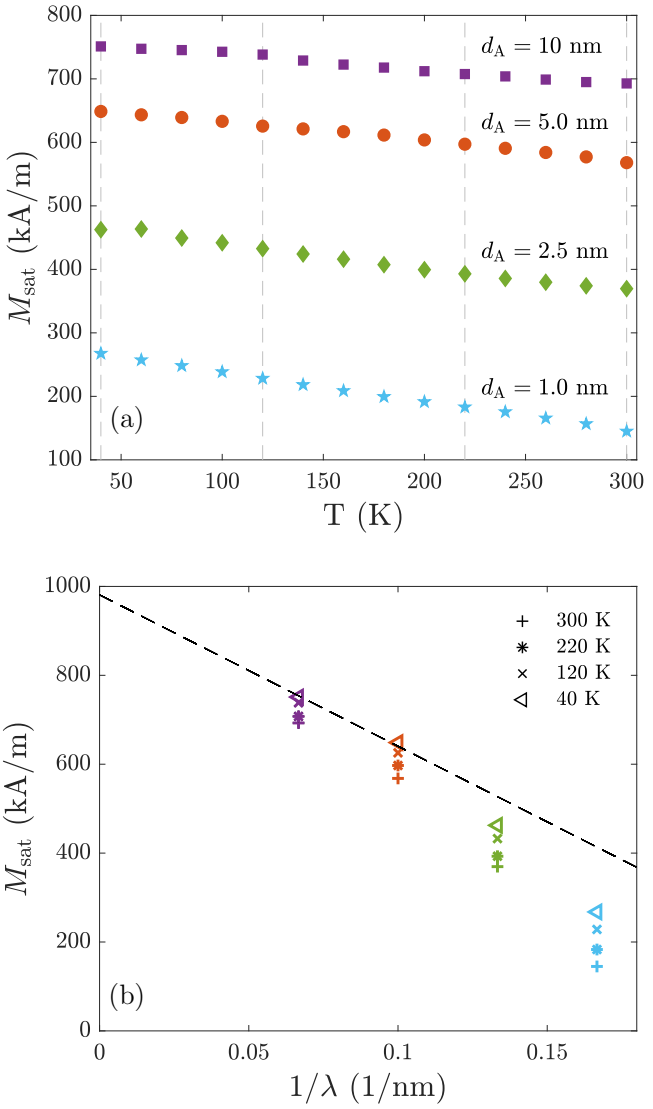

FIG. 4. (a) The magnetization of the A-layer thickness series as a function of temperature. The magnetization decreases monotonously with increasing temperature. (b) The bilayer thickness dependence of the magnetization of the A series for selected temperatures. The magnetization does not vary linearly with thickness over the entire thickness range. The vertical dashed gray lines in (a) mark the temperatures shown in (b).

throughout the A layer, we would arrive at an expression for the average magnetization identical to Eq. (1), but with labels "A" and "B" reversed. However, the magnetization does not scale linearly with the inverse bilayer thickness. The dotted line in the figure shows the simple linear model using the measured bulk value for M_A and the value for M_B extracted from Fig. 3(b), at 40 K. The samples with thicker A layers (5 nm and 10 nm) follow the model well but for smaller thicknesses (1.0 nm and 2.5 nm) the magnetization is lower than expected. This is a sign of a finite-size effect, where the magnetization in layer A is suppressed close to its interfaces [26], as shown schematically in Fig. 2(a). From the thickness where the data diverge from the dotted line, we can infer that the magnetically suppressed interface layer is between 1.25

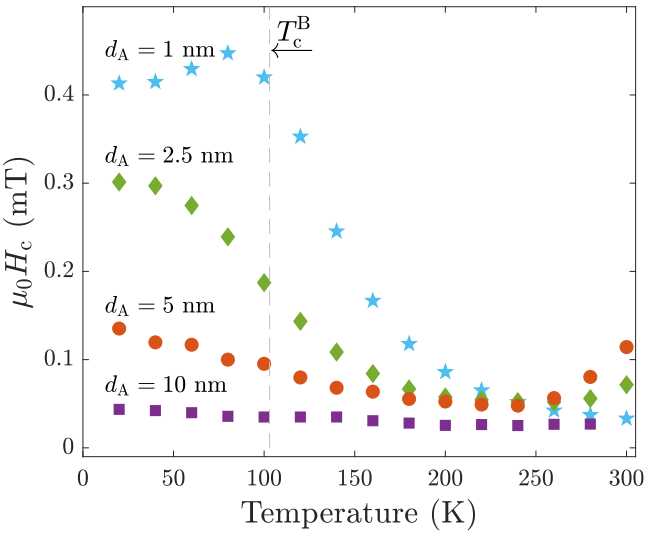

FIG. 5. The coercivity as a function of temperature for the A sample series. The gray vertical line marks the intrinsic T_c^B.

and 2.5 nm in thickness. A similar trend is not observed in the B-layer series since the magnetization at the B-layer side of the interfaces is in all cases enhanced by the proximity to the A layers. It is also worth noting that the magnetic proximity effect actually alters the finite-size effect, since the magnetization in the A layer does not go to zero at the interfaces as it would at an interface with a fully nonmagnetic material.

The temperature dependence of the coercivity of the A-layer series is shown in Fig. 5. In all cases we see a single-step switching, i.e., with both the A and B layers switching simultaneously, as shown in Fig. 2(a). For $d_A = 10$ nm the coercive field is very small (approximately 0.05 mT) and constant throughout the entire temperature range. For smaller d_A the coercive field at 20 K increases due to the decreasing total magnetic moment of the A layers and the decreasing magnetization of the multilayer as a whole. This results in a decreasing torque from the applied field and therefore a higher field is required to switch the magnetization. At higher temperatures the coercive field of these samples decreases until it reaches a similar H_c as for the sample with $d_A = 10$ nm. The drop in H_c occurs in those cases in a temperature region extending well above T_c^B, where for $d_A = 1$ nm the enhancement in coercivity extends up to approximately 200 K.

Above T_c^B the A layers should switch independently of each other and their coercivity be determined by their intrinsic coercivity and finite-size effects. Below T_c^B the coercive field will be governed by the interplay between the coercivity of the B layers and the A layers. The B layers have an unknown coercivity and anisotropy since both properties may be strongly affected by the proximity of the A layers during growth. What we observe is that for thin d_A, the increase in the coercive field extends to much higher temperatures than expected. This must be due to a ferromagnetic ordering and spin stiffness in the intrinsically paramagnetic B layer due to the proximity of the ferromagnetic A layer which is sufficient to alter the overall coercivity of the multilayer.

The VSM measurements suggest that the magnetization of layer B within the multilayer can be well approximated

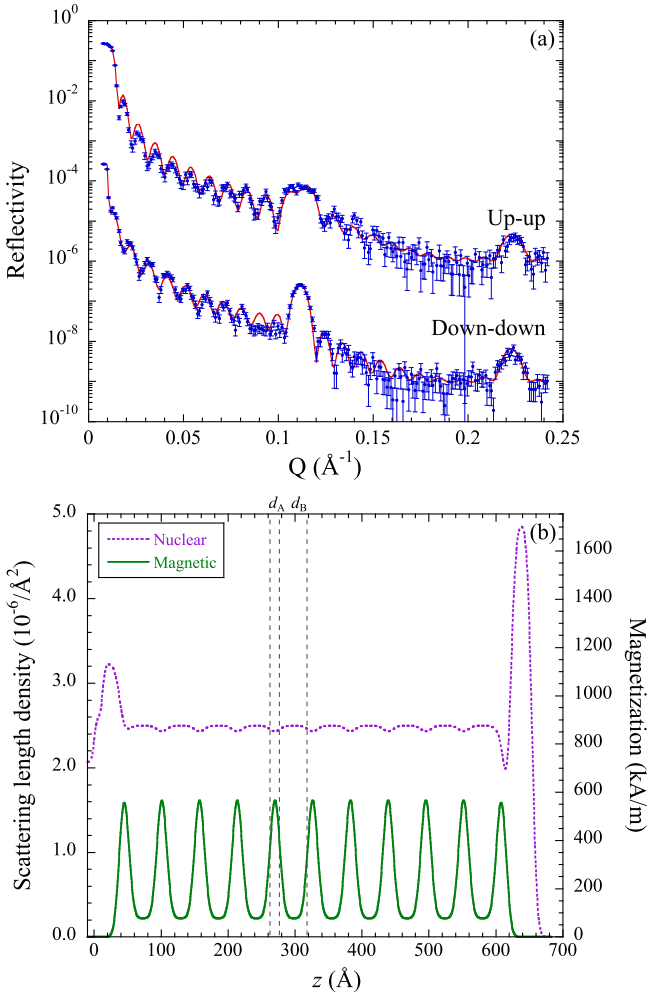

FIG. 6. (a) PNR measurements of the multilayer sample with $d_A = 1.0$ nm and $d_B = 5.0$ nm (blue dots), including fits (red lines), for the up-up and down-down spin channels, taken at 120 K. (b) Nuclear and magnetic scattering length density as a function of depth, producing the fits shown in (a).

by a constant value throughout its thickness. Yet they also show that finite-size effects reduce the magnetization of the A layers close to their interfaces. To investigate the profile of the magnetization in the A and B layers further and confirm the size of the magnetization in layer B, we have carried out PNR measurements. PNR gives depth resolved information about the magnetic moment of the sample and is therefore ideally suited for the study of magnetization profiles in layered structures. The reflectivity curves for the up-up and down-down spin channels are shown in Fig. 6(a) for the sample with nominally $d_A = 1.0$ nm and $d_B = 5.0$ nm, collected at a temperature of 120 K. Clear multilayer (Bragg) peaks are observed corresponding to both the nuclear and magnetic periodicity of the multilayer. Fitting in GenX yields thickness values of 1.3 and 4.3 nm for the A and B layers, respectively, and interface widths of approximately 0.6 nm. In addition, a 1.3 nm SiO_2 is included on the substrate and a 3.2-nm surface oxide on the capping layer. The densities of each layer are fitted and allowed to vary by approximately 10% from the calculated values to allow for the slight reduction in density due to the amorphous structure. This agrees well with the XRR results, although the interface widths are slightly higher in the PNR fit.

The fact that the up-up and down-down spin channels are different shows that there is indeed a magnetic contribution to the scattering length density (SLD). The full nuclear and magnetic SLDs obtained by fitting in GenX are shown in Fig. 6(b) as a function of depth z. A constant magnetization is assumed throughout the B-layers, in line with the simple magnetization model above [Eq. (1)], but the interface roughness is allowed to vary, producing the smoothly changing magnetic SLD across the interfaces. Since there is little nuclear contrast between layers A and B the roughness has a minimal effect on the nuclear SLD, whereas the strong magnetic contrast means that the roughness affects the magnetic SLD strongly. Therefore, although the same interface roughness is applied to both the nuclear and magnetic SLDs, the fitting is more sensitive to the magnetic interface profile than the structural (or nuclear) interface profile. The smoothly varying magnetic SLD is therefore a good approximation of the proximity induced magnetization profile across the interfaces, which explains why the PNR yields slightly higher interface widths than XRR. Nonetheless, layer thicknesses obtained in this way are consistent with XRR measurements and one bilayer is highlighted with the vertical dashed lines in the figure. The model fits the data well and the best fit is obtained with a nonzero moment in the middle of the B layers which confirms that the B layers carry a magnetic moment above T_c^B. The magnetic SLD can be converted to units of magnetization as shown in the figure. By integrating the magnetization over the thickness of layers A and B we can determine that the average magnetization in the layers is $M_A = 510$ kA/m and $M_B = 150$ kA/m. M_A is somewhat lower than the measured bulk value of 980 kA/m due to the finite-size effect and M_B is quite consistent with the value determined by applying the linear model to the VSM data in Fig. 3(b). These values correspond to an average magnetic moment per Co atom of 0.75 μ_B and 0.35 μ_B in the A and B layers, respectively. By integrating over the entire magnetization profile we find that the total magnetization is 230 kA/m which is in good agreement with the magnetization measured by VSM at 120 K.

IV. CONCLUSIONS

The magnetic proximity effect was investigated in multilayered structures of alternating $Co_{60}(Al_{70}Zr_{30})_{40}$ (low T_c) and $Co_{85}(Al_{70}Zr_{30})_{15}$ (high T_c). By fixing the thickness of the high-T_c layer, the range of the induced magnetic ordering due to the proximity effect in the low-T_c layer was determined by VSM measurements. The size of the induced magnetization is approximately constant throughout a 10-nm-thick $Co_{60}(Al_{70}Zr_{30})_{40}$ layer, even at three times its intrinsic ordering temperature T_c^B. However, PNR measurements show that there is an interface region of smoothly varying magnetization between the layers but this region is small compared to the smallest B-layer thickness studied. Although the low-T_c layer carries a magnetic moment in the entire temperature range studied, there are signs of a magnetic phase transition at a temperature somewhat above T_c^B. This indicates that there are two different magnetic phases induced by the proximity effect,

with different temperature dependence and extension. These results demonstrate the intricacies of magnetic proximity effects in amorphous metals and how they can fundamentally alter the behavior of such materials in layered structures. Much is still unknown about the nature of the induced magnetization such as its dynamic properties and the potential for controlling its size and extension with parameters other than temperature. Besides the obvious need to take magnetic proximity effects into account in the design of magnetic nanostructures, there is great potential for using them to enhance the properties of low-T_c materials or for tuning of magnetic properties in heterostructures.

ACKNOWLEDGMENTS

This work was supported by the Icelandic Centre for Research, Grant No. 174271-051, the University of Iceland Research Fund, and the Swedish Research Council (VR).

[1] R. M. White and D. J. Friedman, Theory of the magnetic proximity effect, J. Magn. Magn. Mater. **49**, 117 (1985).
[2] M. J. Zuckermann, The proximity effect for weak itinerant ferromagnets, Solid State Commun. **12**, 745 (1973).
[3] P. K. Manna and S. M. Yusuf, Two interface effects: Exchange bias and magnetic proximity, Phys. Rep. **535**, 61 (2014).
[4] U. Bovensiepen, F. Wilhelm, P. Srivastava, P. Poulopoulos, M. Farle, A. Ney, and K. Baberschke, Two Susceptibility Maxima and Element Specific Magnetizations in Indirectly Coupled Ferromagnetic Layers, Phys. Rev. Lett. **81**, 2368 (1998).
[5] F. Magnus, M. E. Brooks-Bartlett, R. Moubah, R. A. Procter, G. Andersson, T. P. A. Hase, S. T. Banks, and B. Hjörvarsson, Long-range magnetic interactions and proximity effects in an amorphous exchange-spring magnet, Nat. Commun. **7**, 11931 (2016).
[6] R. W. Wang and D. L. Mills, Onset of long-range order in superlattices: Mean-field theory, Phys. Rev. B **46**, 11681 (1992).
[7] N. J. Gökemeijer, T. Ambrose, and C. L. Chien, Long-Range Exchange Bias Across a Spacer Layer, Phys. Rev. Lett. **79**, 4270 (1997).
[8] W. J. Gallagher and S. S. P. Parkin, Development of the magnetic tunnel junction MRAM at IBM: From first junctions to a 16-Mb MRAM demonstrator chip, IBM J. Res. Dev. **50**, 5 (2006).
[9] S. S. P. Parkin, Giant magnetoresistance in magnetic nanostructures, Annu. Rev. Mater. Sci. **25**, 357 (1995).
[10] R. H. Victora and X. Shen, Composite media for perpendicular magnetic recording, IEEE Trans. Magn. **41**, 537 (2005).
[11] C. Song, M. Sperl, M. Utz, M. Ciorga, G. Woltersdorf, D. Schuh, D. Bougeard, C. H. Back, and D. Weiss, Proximity Induced Enhancement of the Curie Temperature in Hybrid Spin Injection Devices, Phys. Rev. Lett. **107**, 056601 (2011).
[12] Q. L. He, X. Kou, A. J. Grutter, G. Yin, L. Pan, X. Che, Y. Liu, T. Nie, B. Zhang, S. M. Disseler, B. J. Kirby, W. Ratcliff II, Q. Shao, K. Murata, X. Zhu, G. Yu, Y. Fan, M. Montazeri, X. Han, J. A. Borchers, and K. L. Wang, Tailoring exchange couplings in magnetic topological-insulator/antiferromagnet heterostructures, Nat. Mater. **16**, 94 (2016).
[13] Z. Jiang, C.-Z. Chang, C. Tang, P. Wei, J. S. Moodera, and J. Shi, Independent tuning of electronic properties and induced ferromagnetism in topological insulators with heterostructure approach, Nano Lett. **15**, 5835 (2015).
[14] P. Wei, F. Katmis, B. A. Assaf, H. Steinberg, P. Jarillo-Herrero, D. Heiman, and J. S. Moodera, Exchange-Coupling-Induced Symmetry Breaking in Topological Insulators, Phys. Rev. Lett. **110**, 186807 (2013).
[15] M. A. Tomaz, W. J. Antel Jr, W. L. O'Brien, and G. R. Harp, Induced V moments in Fe/V(100), (211), and (110) superlattices studied using x-ray magnetic circular dichroism, J. Phys.: Condens. Matter **9**, L179 (1997).
[16] H. Palonen, F. Magnus, and B. Hjörvarsson, Double magnetic proximity in $Fe_{0.32}V_{0.68}$ superlattices, Phys. Rev. B **98**, 144419 (2018).
[17] L. Cheng, Z. Altounian, D. H. Ryan, J. O. Ström-Olsen, M. Sutton, and Z. Tun, Pd polarization and interfacial moments in Pd-Fe multilayers, Phys. Rev. B **69**, 144403 (2004).
[18] W. L. Lim, N. Ebrahim-Zadeh, J. C. Owens, H. G. E. Hentschel, and S. Urazhdin, Temperature-dependent proximity magnetism in Pt, Appl. Phys. Lett. **102**, 162404 (2013).
[19] O. Rader, E. Vescovo, J. Redinger, S. Blügel, C. Carbone, W. Eberhardt, and W. Gudat, Fe-Induced Magnetization of Pd: The Role of Modified Pd Surface States, Phys. Rev. Lett. **72**, 2247 (1994).
[20] C.-M. Choi, J.-O. Song, and S.-R. Lee, Thermal stability of magnetic tunnel junctions with new amorphous zral-alloy films as the under and capping layers, IEEE Trans. Magn. **41**, 2667 (2005).
[21] P. Sharma, H. Kimura, and A. Inoue, Magnetic behavior of cosputtered Fe-Zr amorphous thin films exhibiting perpendicular magnetic anisotropy, Phys. Rev. B **78**, 134414 (2008).
[22] R. Gemma, M. t. Baben, A. Pundt, V. Kapaklis, and B. Hjörvarsson, Consequences of randomness: Compositional contours in amorphous alloys, arXiv:1811.03354.
[23] R. A. Procter, F. Magnus, G. Andersson, C. Sánchez-Hanke, B. Hjörvarsson, and T. Hase, Magnetic leverage effects in amorphous SmCo/CoAlZr heterostructures, Appl. Phys. Lett. **107**, 062403 (2015).
[24] F. Magnus, R. Moubah, A. H. Roos, A. Kruk, V. Kapaklis, T. Hase, B. Hjörvarsson, and G. Andersson, Tunable giant magnetic anisotropy in amorphous SmCo thin films, Appl. Phys. Lett. **102**, 162402 (2013).
[25] H. Raanaei, H. Nguyen, G. Andersson, H. Lidbaum, P. Korelis, K. Leifer, and B. Hjörvarsson, Imprinting layer specific magnetic anisotropies in amorphous multilayers, J. Appl. Phys. **106**, 023918 (2009).
[26] P. T. Korelis, P. E. Jönsson, A. Liebig, H.-E. Wannberg, P. Nordblad, and B. Hjörvarsson, Finite-size effects in amorphous $Fe_{90}Zr_{10}/Al_{75}Zr_{25}$ multilayers, Phys. Rev. B **85**, 214430 (2012).
[27] M. Björck and G. Andersson, GenX: An extensible X-ray reflectivity refinement program utilizing differential evolution, J. Appl. Crystallogr. **40**, 1174 (2007).